MONTHLY VARIABILITY OF RADIO-WAVE PROPAGATION EFFECTS ON SATELLITE LINK OPERATING AT 20 GHz

by

Aimé R.M.M. Itamba

A thesis submitted in partial fulfillment
of the requirements for the degree of
Master in Signal Processing and
Imaging, 60 credits

Department of Physics
Faculty of mathematics
and natural sciences

UiO : Universitetet i Oslo

Spring 2022

UNIVERSITY OF OSLO

Monthly variability of radio-wave propagation effects on satellite link operating at 20 GHz

by

Aimé R.M.M. Itamba

ABSTRACT

Radio wave propagation plays a significant role in the design and ultimate performance of space-to-earth communications systems. Atmospheric constituents, such as gases, clouds, and rain, hamper the reliability of space communications. Rain is the atmospheric phenomena having a predominant effect on satellite communication systems operating at frequencies above 10 GHz, mutually with regards to signal attenuation and wave depolarization. Therefore, rain attenuation has historically come under scrutiny and significant effort has been purposely committed to developing models capable of predicting yearly rain attenuation statistics (see e.g., [1]). Until now, considerably less devotion has been given to the analysis and prediction of monthly rain attenuation statistics, the understanding of which can result to substantial gains in the design and processing of innovative systems exploiting the high spatial and temporal variability of the rainfall process (e.g., design of communication systems for Earth observation missions or of broadcast systems based on worst month rain attenuation statistics). The main interest is to understand how the effects induced by the propagation fluctuate per month over the year. This may allow for link budget for different periods of less than one year, such as the summer months. Presently, the internationally accepted approach implement prediction for an average year and for worst month, but not for single months or a seasonal period less than a year.

In this work, measurement data collected from three different sites in Norway are used to derive monthly statistics, the results of which are compared with corresponding measured or modeled results from the literature. The objective is to derive an estimate for a month or a few consecutive months of measured attenuation exceeding the link margin, with a primary focus on attenuation due to rain only.

Assignment given: November 2021
Supervisor: Terje Tjelta, ITS
Co-supervisor: Sverre Holm, UiO

Table of Contents

ACKNOWLEDGMENTS

First and foremost, I wishe to express my sincere gratitude to Professor Terje Tjelta whose guidance and dedication have helped me immensely in many aspects of this thesis, especially his contribution in providing measurement data and source codes without which this project would not be achieved in due time.

Furthermore, I would also like to thank Professor Sverre Holm for his invaluable insight for the successful completion of this thesis.

Also, I would like to thank Kidist Yisfashewa Wondemu for providing us with the additional data we needed.

Aimé R.M.M. Itamba
Oslo, May 16, 2022

ABBREVIATIONS AND ACRONYMS

Ka-band - frequency band between 17.7 and 21.2 GHz (downlink) and 27-31 GHz (downlink) assigned to satellite communication.

RF - Radio Frequency.

ITU - International Telecommunication Union.

ITU-R - International Telecommunication Union – Radiocommunication Sector.

RMS - Root Means Square.

GPCC - Global Precipitation Climatology Centre

ECMWF - European Centre for Medium-Range Weather Forecast

1. Introduction

1.1. Basic Principles of Satellite and its Importance to Norway

A communication satellite can be described as an artificial earth-orbiting satellite that receives, amplifies, and possibly processes a communications signal from grounded transmitting base stations, then forward it back to the ground for reception by one or multiple base stations. When used as a communication device, information is never emanated nor terminated at the satellite itself, in this case the satellite is merely an active transmission relay, operating in a similar fashion to relay towers employed in terrestrial microwave communications, to assist transmission of information or messages from one point to another through space. This is particularly true for information generated on the earth.

When there is an instrument on the satellite, such as radar, that observe and convey information to an earth station, the configuration is called an Earth observation satellite or Earth remote sensing satellite, this includes spy satellite and others intended for non-military applications such as environmental monitoring, cartography, meteorology and more.

Satellite is one of the most remarkable outcomes of research in communications and space programs whose ambition is the accomplishment of a substantial increase in ranges and capacities for the relay of information in a very broad bundle of telecommunications, meteorological, and scientific applications. These satellite systems depend on the transmission of radio-waves to and from the satellite and rely on the propagation characteristics of the transmission path, mainly the earth's atmosphere. Radio-wave propagation thus plays a decisive role in the design and performance of space communications systems. The engineering aspect of satellite communications combines such diverse topics as antennas, signal processing, data communication, modulation, detection, coding, filtering, orbital mechanics, and electronics. Each is a major field of study, and each has its own extensive literature [2],[3].

Arctic Norway comprises the northernmost parts of Norway. Except for Russia, Norway has Europe's largest area to oversee particularly in the Arctic or the High Arctic region, an area of increasing importance for its natural resources such as fish, gas, and oil. The exploitation of these resources is the main factor for the creation of new sailing routes across this region, and all indications

suggest that this trend will progress into the future, causing concerns regarding safety and rescue in Norwegian waters [4].

Satellite system has proven to be the best communication and monitoring system to screen this region.

And incidentally, it is worth mentioning that the Norwegian polar region of Svalbard has proven to be a well-fitting location for downloading data from polar orbiting Earth observations satellites [5].

1.2. Preliminaries

Satellite link is a wireless communication which is sensitive to atmospheric conditions, hence in the design of Earth-space satellite communication systems, several propagation effects resulting from changes in the atmosphere must be considered to prevent degradation of the wanted signal.
These propagation effects include:

1) attenuation due to atmospheric gases
2) clear-air effects
3) attenuation by precipitation and clouds
4) ionospheric effect

The sum of these different effects constitutes the propagation loss on an Earth-space link, relative to the free-space loss, and may also include other contributions such as:

a. focusing and defocusing.
b. decrease in antenna gain due to wave-front incoherence.
c. attenuation by sand and dust storms.

Each individual contributor has its distinctive attributes as a function of frequency, geographic location, and elevation angle. As a general guideline, at elevation exceeding 10 degrees, mainly attenuation by gases, rain and cloud attenuation and likely scintillation will be meaningful, depending on propagation conditions [3],[6].

1.2.1. Attenuation due to atmospheric gases

Although largely caused by absorption, attenuation by atmospheric gases is based mostly on frequency, elevation angle, altitude or height above sea level and oxygen and water vapour density (absolute humidity). Largely negligible at frequencies sub 10 GHz, but increasingly significant at frequencies above 10 GHz, particularly at small elevation angles. A complete method for calculating gaseous attenuation can be found in Recommendation ITU-R P.676 (method available for the range up to 1 THz).

1.2.2. Clear-air effects

Clear-air effect, which is a term related to higher altitude turbulence commonly associated with wind shear, is described as an unanticipated strong turbulence occurring in cloudless regions, capable of introducing severe impairments of signal and channel availability.

At frequencies less than 10 GHz and at elevation angles exceeding 10^{o}, severe fading caused by clear-air effects in the absence of precipitation are improbable. But at small elevation angles ($\leq 10^{o}$) and at higher frequencies over 10 GHz, however, tropospheric scintillation can occasionally induce severe deterioration in performance. At very small elevation angles ($\leq 4^{o}$ on inland paths, and $\leq 5^{o}$ on over-water or coastal paths), deterioration caused by multipath propagation effects can be notably stringent. At some locations, ionospheric scintillation may be critical at frequencies beneath about 6 GHz (see Recommendation ITU-R P.531).

1.2.3. Scintillation

Scintillation is a clear-air effect defined as the state of accelerated fluctuations of a radio-wave's signal parameters produced by time dependent inconsistency in the transmission path.

Scintillation effects can be generated in both ionosphere and in the troposphere. Electron density variations taking place in the ionosphere can influence frequencies up to around 6 GHz, while refractive index variations occurring in the troposphere induce scintillation effects in the frequency band greater than 3 GHz.

The amplitude of tropospheric scintillation relies upon the significance and configuration of the refractive index variation along the propagation path. Amplitude scintillation augment as a function of frequency and with the path length and decline as the antenna beamwidth reduces because of aperture averaging [3].

1.2.4. Ionospheric effects

Signal transmission between ground base and satellites is altered by space weather due to disturbances in the ionosphere, which can reflect, refract or absorb radio waves. Space weather can alter the density structure of the ionosphere creating areas of increase density. This alteration of the ionosphere can make the transmission less precise and may lead to total loss of the signal. Because the ionosphere can act as a lens or a mirror to radio waves passing through it [7].

1.3. Prediction Methods of Annual Rain Attenuation

Many models have been proposed in the literature to provide the prediction of annual statistics of attenuation owing to a given atmospheric factor. In this section, different approaches for rain attenuation are briefly mentioned.

1.3.1. Rain attenuation models

Rain droplets absorb and scatter the signal energy causing its level of intensity to dissipate to a value depending on the size, magnitude, and form of the droplets passed through by the signal as well as the rain rate. Rain usually occurs at different heights above sea level depending on the region of the earth.

1.3.2. Earth-space satellite link

Actual earth-space models can be grouped into five taxonomies depending on the configuration of the rain attenuation method. These comprise the empirical, physical, statistical, and optimization-based methods.

- Empirical model: The model is founded on experimental data measurements rather than input-output interrelations that can be methodically outlined. The model is then categories as an empirical category.

- Physical model: The physical model is built on some of the correlations between the rain attenuation model's framework and the physical structure of rain events.

- Statistical model: This method is based on statistical weather and infrastructural data analysis, and the ultimate model is achieved because of regression analysis in most cases.

- Optimization-based model: In this type of model, the input parameters of some of the other factors that affect the rain attenuation are developed through optimization (e.g., minimum error value) process.

As a second order model we can name the Fade slope model, where the slope of attenuation from the rain attenuation versus time data are developed with a particular experimental setup. Later, these data are used to predict rain attenuation.

It should be mentioned that prediction methods use both physical and empirical models along with some statistical distribution. In this work the focus is on statistical method for the prediction of monthly rain attenuation.

2. Statistical Method

2.1 ITU-R Method

In this section, the generic method to predict attenuation caused by precipitation and clouds along a slant propagation path for the design of earth-space satellite link is described first, next the case of rain attenuation along a slant path is presented.

The principal factor when considering attenuation caused by rain, is that the attenuation it causes increases with rainfall rate, with frequency typically up to around 100 GHz where it then remains at that level, and with decreasing elevation angle. Rain attenuation can normally be neglected at frequencies below about 5 GHz.

To predict the attenuation distribution due to precipitation along a slant path, it is necessary to obtain system and climate data, then the space and time descriptions can be established. A general method developed by the ITU-R for calculating attenuation is presented below.

2.2. Estimation of Long-Term Statistics of Rain Attenuation

The following strategy assesses the long-term statistics of the slant-path rain attenuation at a given point for frequencies up to 55 GHz. The following parameters are needed:

$R_{0.01}$: point rainfall rate for the location for 0.01% of an average year (mm/h)

h_s: height above mean sea level of the earth station (km)

θ: elevation angle (degrees)

φ: latitude of the earth station (degrees)

f: frequency (GHz)

R_e: effective radius of the Earth (8500 km).

The geometry is illustrated in **Figure1,** where:
A = frozen precipitation, B = rain height, C = liquid precipitation, and
D = Earth-space path.

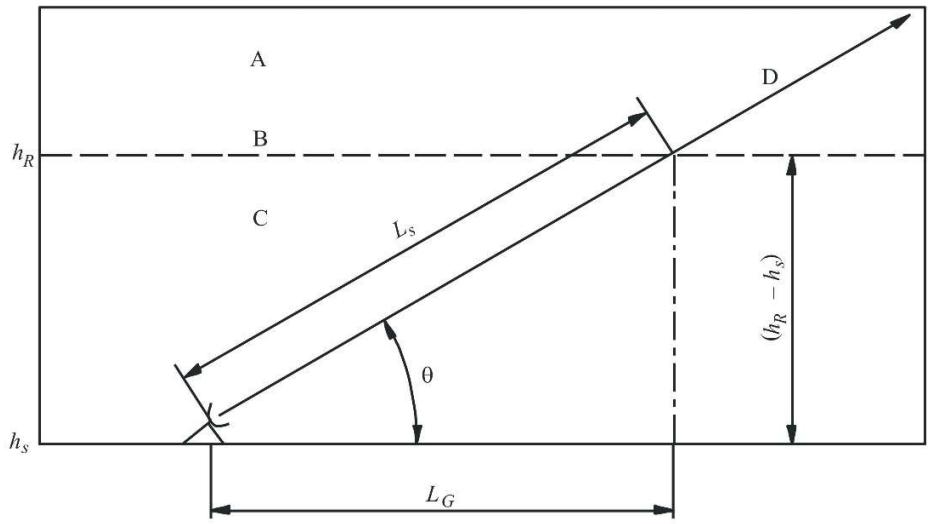

Figure 1: Schematic presentation of an Earth-space path giving the parameters to be input into the attenuation prediction process. (Picture reference ITU-R rec. P-618-13[6])

The current approach formulated by the ITU-R recommendation P.618-13, is composed of the following steps 1 to 9 to predict the attenuation exceeded for 0.01 % of the time, and step 10 for other time percentages.

Step 1: Determine the rain height, h_R, as given in Recommendation ITU-R P.839

$$h_R = h_o + 0.36 \text{ km} \quad (1)$$

Noting that for areas of the Earth where no specific information is obtainable, the mean annual 0° C isotherm height above mean sea level, h_o, is a component part of this guideline and is available in the form of a digital map provided in the file R-REC-P.839-4-201309-I!!ZIP-E.zip.

Step 2: For $\theta \geq 5^{o}$ the slant-path length, L_s, below the rain height is computed from:

$$L_S = \frac{(h_R - h_S)}{\sin\theta} \quad \text{km} \tag{2}$$

For $\theta < 5°$ a more rigorous formula is used, that is:

$$L_s = \frac{2(h_R - h_S)}{(\sin^2\theta + 2(h_R - h_S)/R_e)^{1/2} + \text{si}} \text{ km} \tag{3}$$

Where, R_e = radius of the earth = 6378 km. Note that if $(h_R - h_s)$ is less than or equal to zero, the predicted rain attenuation for any time percentage is zero and the next steps are not necessary.

Step 3: The horizontal projection, L_G, of the slant-path length is calculated from:

$$L_G = L_s \cdot \cos\theta \text{ km} \tag{4}$$

Step 4: Obtain the rainfall rate, $R_{0.01}$, exceeded for 0.01% of an average year (with an integration time of 1 min). If this long-term statistic is unavailable from local data sources, an estimate can be procured from the maps of rainfall rate given in Recommendation ITU-R P.837. If $R_{0.01}$ is equal to zero, the predicted rain attenuation is zero for any time percentage and the following steps are not required.

Step 5: Obtain the specific attenuation, γ_R, using the frequency-dependent coefficients given in Recommendation ITU-R P.838 and the rainfall rate, $R_{0.01}$, determined from Step 4, by using:

$$\gamma_R = k\left(R_{0.01}\right)^{\alpha} \tag{5}$$

Step 6: The 0.01%-time horizontal reduction factor, $r_{0.01}$, can be calculated by the following formula:

$$r_{0.01} = \frac{1}{1+0.78\sqrt{\frac{L_G \cdot \gamma_R}{f}} - 0.38(1-e^{-2L_G})} \tag{6}$$

Step 7: Calculate the vertical adjustment factor, $\nu_{0.01}$, for 0.01% of the time:

$$\zeta = \tan^{-1}\left(\frac{h_R - h_S}{L_G \cdot r_{0.01}}\right) \quad \text{degrees}$$

For $\zeta > \theta$ $\qquad L_R = \frac{L_G \cdot r_{0.01}}{\cos\theta}$ km

Else, $\qquad L_R = \frac{(h_R - h_S)}{\sin\theta}$ km

if $|\varphi| < 36^o$, $\qquad \chi = 36 - |\varphi|$ degrees

Else, $\qquad \chi = 0$ degrees

$$\nu_{0.01} = \frac{1}{1+\sqrt{\sin\theta}\left(31\left(1-e^{-(\theta/(1+\chi))}\right)\frac{\sqrt{L_R\gamma_R}}{f^2} - 0.45\right)} \tag{7}$$

Step 8: The effective path length is:

$$L_E = L_R \cdot \nu_{0.01} \quad \text{km} \tag{8}$$

Step 9: The predicted attenuation exceeded for 0.01% of an average year is computed from:

$$A_{0.01} = \gamma_R \cdot L_E \qquad \text{km} \tag{9}$$

Step 10: The estimated attenuation to be exceeded for other percentages of an average year, in the range 0.001% to 5%, is determined from the attenuation to be exceeded for 0.01% for an average year:

If $p \geq 1\%$ or $\lvert\varphi\rvert \geq 36^\circ$:	$\beta = 0$
If $p < 1\%$ and $\lvert\varphi\rvert < 36^\circ$ and $\theta \geq 25^\circ$:	$\beta = -0.005\left(\lvert\varphi\rvert - 36\right)$
Otherwise:	$\beta = -0.005\left(\lvert\varphi\rvert - 36\right) + 1.8 - 4.25\sin\theta$

$$A_p = A_{0.01}\left(\frac{p}{0.01}\right)^{-\left(0.655 + 0.033\ln(p) - 0.045\ln(A_{0.01}) - \beta(1-p)\sin\theta\right)} \qquad \text{dB} \tag{10}$$

This method provides an estimate of long-term statistics of attenuation caused by rainfall. When comparing measured statistics with the prediction, allowance should be given for quite large year-to-year changes in rainfall rate statistics (see Recommendation ITU-R P.678).

2.3. Rainfall Rate Prediction Method

Rainfall rate stats with a 1-min integration time are needed for the prediction of rain attenuation in Earth-space links as shown in Recommendation ITU-R P.618.

When good long-term local rainfall rate data is not accessible the Recommendation ITU-R P.837-7 [8] provides a method for prediction of rainfall rate statistics with a 1-min integration time. The total monthly data generated by the Global Precipitation Climatology Centre (GPCC) and the monthly mean surface temperature data from the European Centre for Medium-Range Weather Forecast (ECMWF) form the basis for this method.

When long-term local rainfall rate data is accessible with integration times exceeded 1-min, Annex 2 of this same Recommendation has an appropriate approach for converting rainfall statistics with integration times that exceed 1-min to rainfall rate statistics with a 1-min integration time.

The following input parameters are required:

p: Desired annual probability of exceed (%)

Lat: Latitude of the desired location (degrees, N)

Lon: Longitude of the desired location (degrees, E)

Output parameter:

Rp: Rainfall rate exceeded for the desired probability of exceed (mm/h).

Step 1: For each month of the year, define the month number, ii, and the number of days in each month, N_{ii}, as follows:

Month	**Jan**	**Feb**	**Mar**	**Apr**	**May**	**Jun**	**Jul**	**Aug**	**Sep**	**Oct**	**Nov**	**Dec**
ii	01	02	03	04	05	06	07	08	09	10	11	12
N_{ii}	31	28.25	31	30	31	30	31	31	30	31	30	31

Table 1: Number of days in each month.

Step 2: For each month number, *ii*, where *ii* = {01, 02, 03, 04, 05, 06, 07, 08, 09, 10, 11 and 12}, determine the monthly mean surface temperatures, T_{ii} (K), at the desired location (*Lat, Lon*) from reliable long-term local data.

If reliable long-term local data is not available, the monthly mean surface temperatures, T_{ii} (K), at the desired location (*Lat, Lon*) can be obtained from the digital maps of monthly mean surface temperature in Recommendation ITU-R P.1510.

Step 3: For each month number *ii*, where *ii* = {01, 02, 03, 04, 05, 06, 07, 08, 09, 10, 11 and 12}, determine the monthly mean total rainfall, MT_{ii} (mm), at the desired location (Lat, Lon) from reliable long-term local data.

If reliable long-term local data is not available, the monthly mean total rainfall at the desired location (*Lat, Lon*) can be determined from the digital maps of monthly mean total rainfall, MT_{ii} (mm), provided as an integral part of this Recommendation as follows:

1) determine the four grid points (*Lat 1, Lon 1*), (*Lat 2, Lon 2*), (*Lat 3, Lon 3*) and (*Lat 4, Lon 4*) surrounding the desired location (*Lat, Lon*).

2) determine the monthly mean total rainfall, $MT_{1,ii}$, $MT_{2,ii}$, $MT_{3,ii}$, and $MT_{4,ii}$ at the four surrounding grid points of the maps provided with this Recommendation;

3) determine MT_{ii} at the desired location (*Lat, Lon*) by performing a bi-linear interpolation using the four surrounding grid points as described in Annex 1 Paragraph 1b of Recommendation ITU-R P.1144.

Step 4: For each month number, *ii*, convert T_{ii} (K) to t_{ii} (°C).

Step 5: For each month number, *ii*, calculate r_{ii} as follows:

$$\begin{aligned} r_{ii} &= 0.5874 e^{0.0883 \times t_{ii}} \quad && for \quad t_{ii} \geq 0^{\circ} C \\ r_{ii} &= 0.5874 \quad && for \quad t_{ii} < 0^{\circ} C \end{aligned} \qquad (mm/hr) \tag{11}$$

Step 6a: For each month number, *ii*, calculate the monthly probability of rain as follows:

$$P_{0_{ii}} = 100 \frac{MT_{ii}}{24 \times N_{ii} \times r_{ii}} (\%) \tag{12}$$

Step 6b: For each month number, *ii*, if $P_{oii} > 70$, set $P_{oii} = 70$ and

$$r_{ii} = \frac{100}{70} \times \frac{MT_{ii}}{24 N_{ii}}$$

Step 7: Calculate the annual probability of rain, $P_{o\ annual} = P(R>0)$ as follows:

$$P_{0_{annual}} = \frac{\sum_{ii=1}^{12} N_{ii} \times P_{0_{ii}}}{365.25} \quad (\%) \tag{13}$$

Step 8: If the desired rainfall rate probability of exceedance, p, is greater than annual P_0, the rainfall rate at the desired rainfall rate probability of exceedance, R_p, is 0 mm/hr.

If the desired rainfall rate probability of exceedance, p, is less than or equal to annual P_0, adjust the rainfall rate, R_{ref}, until the absolute value of the relative error between the annual rainfall rate probability of exceedance, $P(R > R_{ref})$, and the desired rainfall rate probability of exceedance, p, is less than 0.001% (i.e. until $100 \left| \frac{P(R > R_{ref})}{p} - 1 \right| < 0.001$), where:

$$P\left(R > R_{ref}\right) = \frac{\sum_{ii=1}^{12} N_{ii} P_{ii}\left(R > R_{ref}\right)}{365.25} \quad (\%) \tag{14}$$

$$P_{ii}\left(R > R_{ref}\right) = P_{0_{ii}} Q\left(\frac{\ln\left(R_{ref}\right) + 0.7938 - \ln\left(r_{ii}\right)}{1.26}\right) \quad (\%) \tag{15}$$

And

$$Q(x) = \frac{1}{\sqrt{2\pi}} \int_{x}^{\infty} e^{-\frac{t^2}{2}} dt \tag{16}$$

3. Measurement Stations

3.1. Sites Details

As part of the project called:
KA-BAND RADIO CHARACTERISATION FOR SATCOM SERVICES IN ARCTIC AND HIGH LATITUDE REGIONS, three measurement sites where carefully selected. On the northernmost area, a region whose climate is influenced by a maritime airflow from the ocean, two regions are chosen; **Røst** on a small island, and **Vadsø**, see **Figure 2**. The station of **Nittedal** on the southern part of Norway is also added.

3.2. Assessment of the Selected Locations

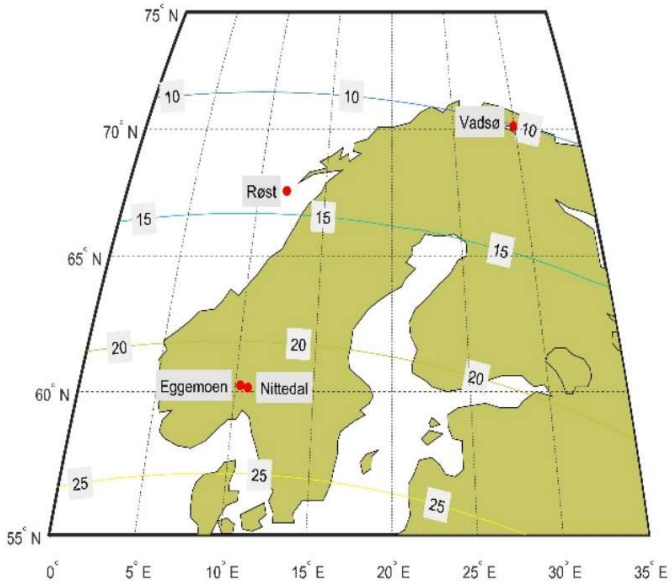

Figure 2: Map with elevation angles indicating the selected measurement locations. (Figure courtesy of Prof. Terje Tjelta, ITS)

The climate of **Røst** can be described as subpolar oceanic, with cold icy winters and brisk summers. Wind is intermittent, and can be heavy at times, notably from October to March. The suburb is located on the small island of Røstlandet, in the southern part of Lofoten islands, at the 67 th parallel. It is just about 115 km north of the Arctic Circle, and along with its neighbouring island of Værøy, it is the only
site in the world north of the Polar Circle to have an average temperature of the coldest month beyond freezing.
The coldest month (February) averages the temperature of 1.1 ºC, and that of the warmest month (August) is of 11.9 ºC. The yearly average rain intensity amount to 15.6 mm/h at 0.01 % of the time [15].

In **Vadsø**, the summers are brief, cool, and usually cloudy and experience freezing, snowy, windy lengthy winters and overcast. Over the course of the year, the thermal reading ordinarily range from -11.1 ºC to 14.4 ºC. An annual average rainfall magnitude of 12.7 mm/h is predicted for 0.01% of time.
Vadsø is situated on the Varanger peninsula near the sea level. The Earth-space path run across a fjord, allowing littoral climate measurements with a range of precipitation forms and probable atmospheric anomalies [16].

At 60º N latitudes the site of **Nittedal** has been chosen. The highest average temperature in Nittedal is 20 ºC in July and the lowest is -3 ºC in January, and an average annual precipitation of 81.72mm. Nittedal has the continental climate prevailing [10].

Location	**Latitude (ºN)**	**Longitude (ºE)**	**Altitude (m)**	**Elevation angle (º)***
Nittedal	**60.1**	**10.8**	**200**	**21.8**
Røst	**67.5**	**12.1**	**10**	**14.1**
Vadsø	**70.1**	**29.7**	**30**	**10.1**

*: Elevation angles are the geometrical ones.
Table 2: Measurement location data and elevation angles towards Ka-Sat.

Location	h_o **(km)**	L **(km)**	**Norway** $R_{0.01}$ **(mm/h)**	**ITU-R** $R_{0.01}$ **(mm/h)**	**Measured** $R_{0.01}$ **(mm/h)**	**Error (dB)**
Nittedal	2.13	5.63	25.5	28.1	33.0	0.0
Røst	0.52	3.53	16.4	41.7	17.9	-1.3
Vadsø	2.0	13.12	12.7	18.2	10.6	1.7

Table 3: Measurement locations, zero-degree height (h_o), slant-path length (L), and rain rate data.

3.3. Measured Parameters

The parameters measured at all stations are as follows:

- Rainfall rate [mm/h]
- Hail [Hits/cm^2]
- Air temperature [^{o}C]
- Air relative humidity [%]
- Atmospheric total pressure [hPa]
- Wind speed [m/s]
- Wind direction [^{o}]
- Signal plus noise power within the noise bandwidth [W]
- Noise floor [W/Hz]

3.4. Rain Attenuation on a Yearly Basis for the Locations

The MATLAB software was used to estimate propagation degradation due to rain according to ITU-R recommendation P.618-13, **Figure 3**.
Later this prediction will be compared with the measured rain attenuation.

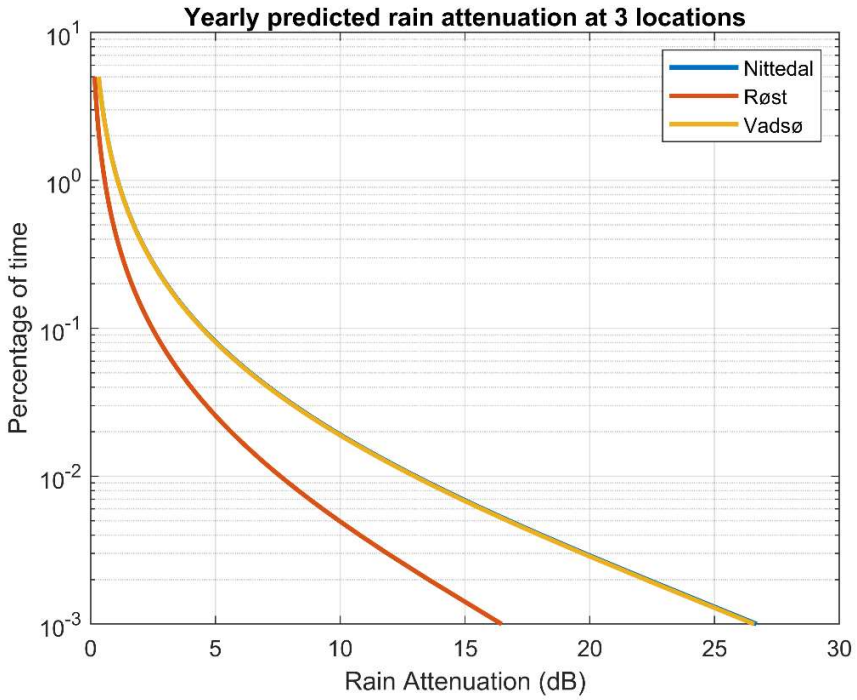

Figure 3: CCDF of yearly predicted rain attenuation for chosen sites.

3.5. Rainfall Rate on a Monthly Basis for the Locations

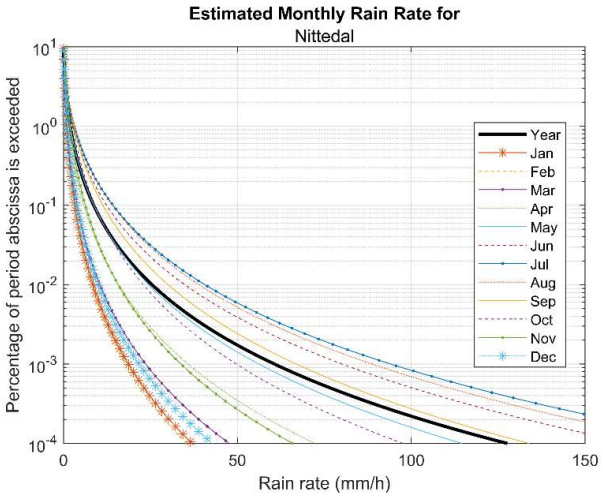

Figure 4a: Predicted monthly rainfall rate based on ITU-R Rec.837-7 for Nittedal.

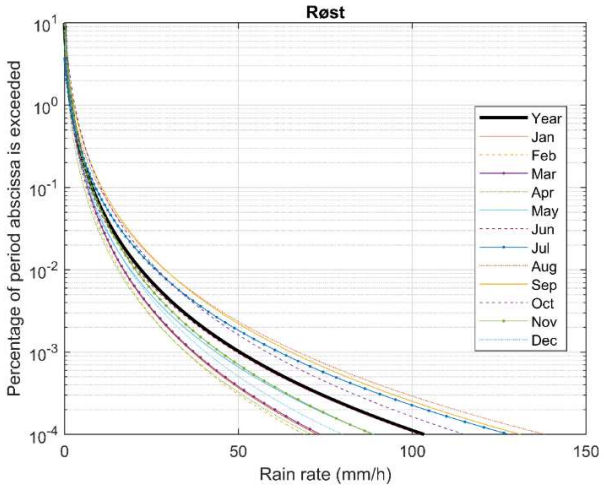

Figure 4b: Predicted monthly rainfall rate based on ITU-R Rec.837-7 for Røst.

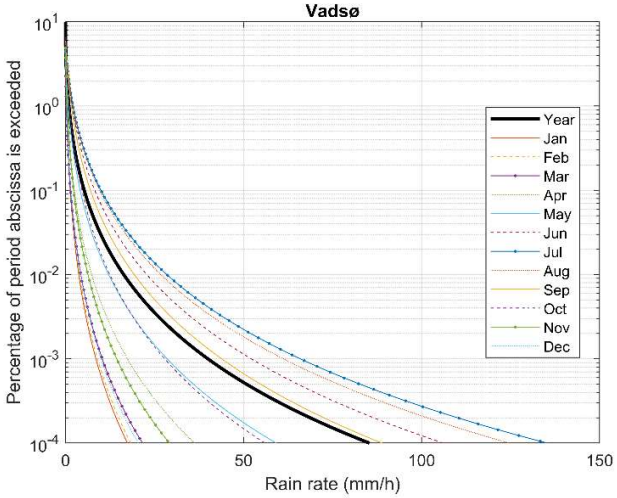

Figugure 4c: Predicted monthly rainfall rate based on ITU-R Rec.837-7 for Røst.

The predicted monthly cumulative distribution of rainfall rate for Nittedal, Røst and Vadsø using ITU-R Rec. 837-7 [8] er presented in **Figures 2 (a – c).**

4. Prediction of Rain Attenuation on Monthly Basis

The main objective of this work is to present a comprehensive methodology for the prediction of monthly tropospheric attenuation with an emphasis on rain attenuation. The task is motivated by the desire to better understand hydrometeor precipitation variability effects on propagation per month over the course of a year.

4.1. The Purpose of Month-to-Month Impairment Prediction

The analysis of the variability of the main tropospheric phenomena (gaseous absorption, clouds, and rain attenuation) and the capability of predicting the magnitude of fade on a monthly scale play a decisive role in the sizing of a direct-to-home (DTH) satellite services.
Considering that DTH satellite payload constitute one of the best remunerative satellite services, as the needed power transmitted by the transponder is set by the results of a link budget which could be determined by the worst rain attenuation conditions (in Ku and Ka bands).

Moreover, short-term temporal variability and fade dynamic are essential to model fade mitigation methods for instance:

- uplink power control
- adaptive coding and modulation

While longer-term performance (yearly, seasonal) is required to anticipate variability within the year of the predictions obtained from models on yearly basis.

4.2. An Overview of the Proposed Methodology

One of the methodologies proposed in academic writing (Luini, Capsoni, Riva & Emiliani, 2015) is to merge some models that have been initially suggested in the literature to provide the prediction of yearly statistics of attenuation owing to a particular atmospheric constituent but, by virtue of the substantial physical principals which they depend on, have been broadened to include monthly time scale by merely providing monthly inputs as opposed to yearly. One such proposed methodology is referred to as monthly attenuation statistics prediction (MASP) Luini et al., 2015, it combines physically sound models for the estimation of fade caused by rain, clouds, or gases to predict total attenuation.

The present work adopts the same strategy and assume that, although the rain attenuation method given by the ITU-R recommendation P.618-13 was developed for the prediction of yearly rain attenuation statistics, it can be utilised for the assessment of monthly rain attenuation statistics, if appropriate inputs, for instance monthly rain intensity and monthly rain height are employed. Afterwards, a comparative analyse is performed to establish validity of this assumption against the measured rain attenuation at the three stations: Nittedal, Røst, and Vadsø, over three consecutive years, from 2013 to 2016.

4.2.1. Monthly rain height

The ITU-R recommendation P.889 stipulates the incidence of rain at diverse heights above sea level related to various regions of the Earth (see step1, Section 2.2.). It gives the average annual 0ºC isotherm height above the mean sea level (h_o) to evaluate the mean annual rain height above the mean sea level (h_R) from the equation:

$$h_R = h_o + 0.36 \text{ km} \quad (17)$$

To derive the monthly rain height (h_{Rm}), a typical process of temperature lapse rate [8] of - 6 degrees/km is used for the zero-degree isotherm height (h_o), that is for the rate of temperature change observed during upward motion through the Earth's atmosphere, the lapse rate is considered positive when temperature decreases with elevation, it is zero when temperature is constant, and in the case temperature increases with elevation, lapse rate is considered as negative. If the upward movement through the Earth's atmosphere is considered as a geometric slant path, the equation of a straight line can be used to derive an expression for the monthly isotherm height as follow:

$$h_{0m}\left(km\right)=\frac{t_m-273.15}{6} \tag{18}$$

Consequently, the monthly rain height is given by:

$$h_{Rm}\left(km\right)=h_{om}+0.36\text{ km} \tag{19}$$

Note that for $h_{om}\leq 0$, h_{om} is set to zero in the above equation.

4.3. Rain Rate Data Distributions

To predict the rain attenuation at a particular location, useful rainfall distribution at the site is required. In this project, three set of data are experimented on using ITU-R data, SEKLIMA data and ERA5 data.

ITU-R rainfall rate distribution rely on the integration time used in finding the rainfall rates. A long-term survey with 1 minute integration time should be used. If long-term locally measured data are not available, then estimates can be acquired from maps of rainfall rate available in Recommendation ITU-R P.837-7[9]. Greater integration time rainfall rate is not utilized by virtue of its failure to capture high intensity short duration rainfall and hence it is discouraged for communication system design.

The SEKLIMA data provided by the Norwegian Meteorological Institute (MET Norway, available at seklima.met.no) is a long-term local data based on monthly mean temperature.

ERA5 which replaces the ERA-interim reanalysis, is the fifth issue ECMWF reanalysis for the world climate and weather for the past 4 to 7 decades. Reanalysis merges model data with measurements from across the world into a globally integrated dataset using the laws of physics. This principle, termed data assimilation, is grounded on the approach used by numerical weather prediction centres, a preceding forecast is coupled with recently obtained observations to yield a better estimate of the state of atmosphere [12].

4.3.1. Monthly rain rate distributions for Nittedal

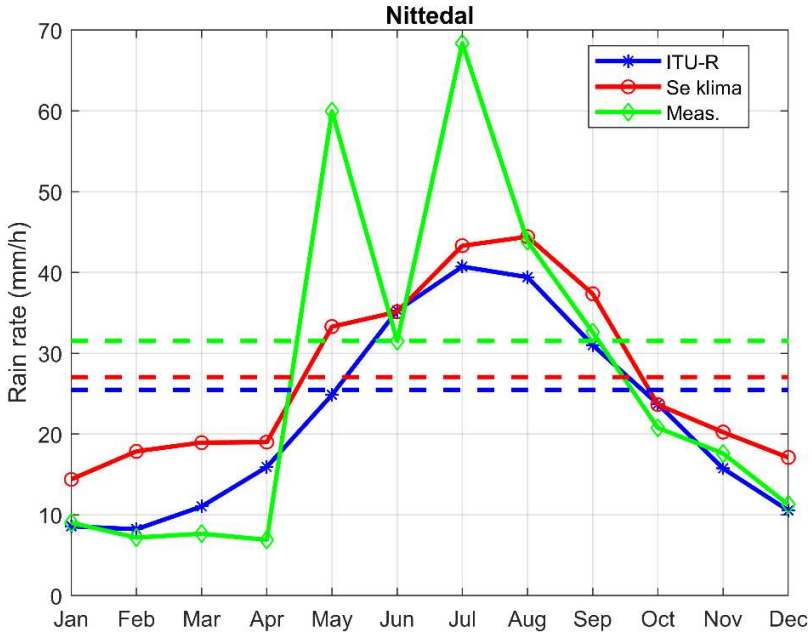

Figure 5: Comparison of monthly mean rain rate with ITU-R data, SEKILIMA data and MEASURED data at Nittedal. The dashed lines show the yearly mean values.

The average monthly rainfall rate received in a tree-years period at Nittedal measurement site is shown in **Figure 5** in comparison with ITU-R and SEKLIMA data respectively. Although, the three data sets seem not to follow the same exact path, it is obvious that they share the same trend with low values in **winter**: December, January and February. In **spring**: Mars, April and May, the same trend of lower rain rates values is observed through Mars and April, but in May the trend shows a noticeable increase of the rain rate for all data sets. The measured value for May is very high reaching a rain rate of 60 mm/h, while the SEKLIMA value deviates from the measurement by 27 mm/h and 34.5 mm/h for ITU-R. In **summer**: June, July and August, the highest values for all the data sets are observed where the measured rain rate reach a peak of 68.3 mm/h while, SEKLIMA and ITU-R equal 43.3 mm/h and 40.7 mm/h respectively. In **autumn**: September, October and November, all the data sets show a coherent decrease in their respective values.

4.3.2. Monthly rain rate data distributions for Røst

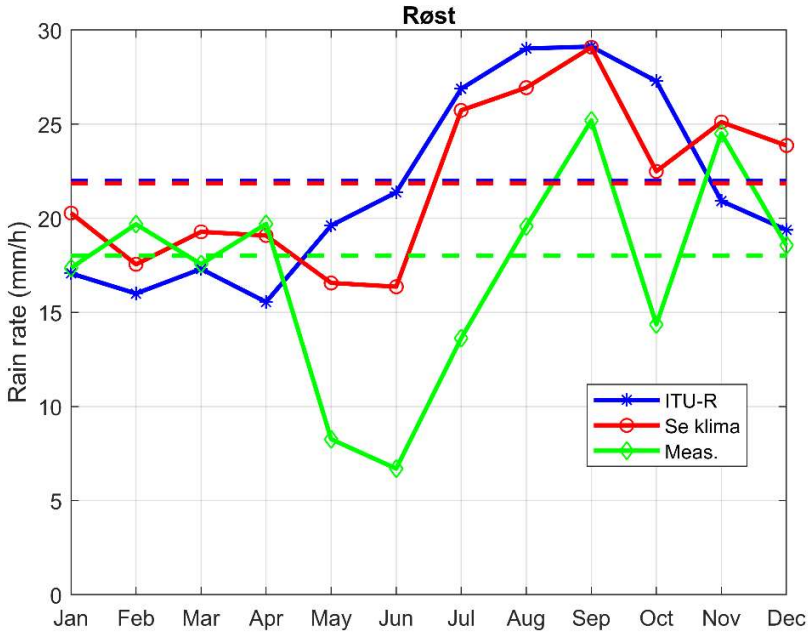

Figure 6: Comparison of monthly mean rain rate with ITU-R data, SEKILIMA data and MEASURED data at Røst. The dashed lines show the yearly mean values.

For the case of Røst, the average monthly rain rate distribution for the three data sets is illustrated in **Figure 6** where an identical tendency of lower values can be noticed for all data sets in the cold months: December, January and February. The same tendency is observed in the two first months of **springtime**: Mars and April. But in May a low value of 8.26 mm/h is registered for the measured rain rate, in contrast to the 19.61 mm/h for ITU-R data and 16.56 mm/h for SEKLIMA data. In **summer**: June shows a moderate increase for ITU-R rain rate of 21.37 mm/h, an unchanged SEKLIMA value from the previous reading and the lowest value of 6.7 mm/h for the measured rain rate. In **autumn**: September reveals coinciding values for ITU-R data and SEKLIMA data at 29.07 mm/h while the measured data is smaller, 25.2 mm/h. In October all the data decrease with various amounts, 27.27 mm/h, 22.49 mm/h and 14.36 mm/h for ITU-R, SEKLIMA and measured respectively. November shows a somewhat increase of roughly the same amount for measured and SEKLIMA rain rate while ITU-R rate is further decreased.

4.3.3. Monthly rain rate data distributions for Vadsø

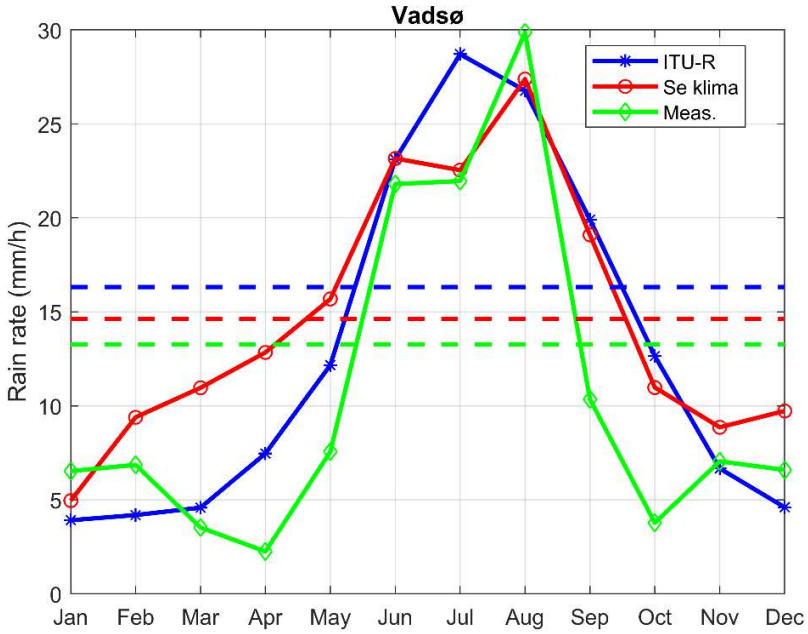

Figure 7: Comparison of monthly mean rain rate with ITU-R data, SEKILIMA data and MEASURED data at Vadsø. The dashed lines show the yearly mean values.

The rain rate distribution at Vadsø is shown in **Figure 7** where the trend for the four temperate seasons do not follow the exact same path but has the same tendency with lower values in **winter**, increasing values in **spring**, the highest values in **summer** and decreasing values in **autumn**. In Vadsø, the lowest rain rate is measured in April while the highest rain rate is measured in August.

4.4. Testing Variable for Comparing Predictions

This section provides an overview of the method for testing the prediction as determined in the fascicle [14] from ITU-R.

This ITU-R document recommends the models undergoing test to be inspected with respect to three conditions: best performance in terms of testing variable, “physical basis” of the method chosen and “simplicity”. Although the three criteria are crucial, in this work the analysis is focused on the first requirement

4.4.1. Principles of the methodology

Typically, attenuation predictions are made for various transmission paths at some set of probability levels. Data for comparing prediction methods is organized at predetermined probability levels, such as 0.001%, 0.01% and 0.1% of the year. For each path, the ratio between the predicted attenuation and the measured attenuation is determined. The natural logarithm of the ratios is applied as a test variable. The effects of other contributing attenuation sources and measurement errors, which mainly influence the lower attenuation values, are compensated by multiplying the logarithm by a scaling factor for measured attenuation values bellow 10 dB. It should be noted that this scaling factor is in fact a power function of the calculated attenuation.

4.4.2. Procedure

All steps are summarized as follows:

a) For each percentage of time, compute the ratio between the predicted attenuation, Ap (dB), and the measured attenuation, Am (dB), for each radio link:

$$S_i = \frac{A_{p,i}}{A_{m,i}} \tag{20}$$

Where S_i is the above calculated ratio for each radio link.

b) Next compute the test-variable V:

$$V_i = \ln S_i \left(\frac{A_{\mathrm{m},i}}{10} \right)^{0.2} \qquad \text{for } A_{m,i} < 10 \text{ dB} \tag{21}$$

$$V_i = \ln S_i \qquad \text{for } A_{m,i} \geq 10 \text{ dB} \tag{22}$$

c) Once the above equation has been computed and repeated for each percentage of time, calculate the mean μ_V, standard deviation σ_V, r.m.s. value ρ_V of the V_i values for each percentage of time:

$$\rho_V = \left(\mu_V^2 + \sigma_V^2 \right)^{0.5} \tag{23}$$

When differentiating the measured attenuation values with the prediction models, the model leading to the lowest values for the statistics cited above is the best one, considering the rain attenuation testing variable criterion. It should be noted that in this work, a single model is provided and used on monthly data averaged over a three-year period.

NOTE 1 – (Weighting function). If some measured distributions are multi-year (n years) data then calculate the mean μ_V, standard deviation σ_V, and r.m.s. value ρ_V, of the n V_i values (e.g., if the average year data from three years of observation are assessed, then use three times the same V_i value for each percentage of time).

NOTE 2 – (Assessment over decades of probability levels). For the assessment of prediction methods over decades of probability levels (e.g. from 0.001% to 0.1% of time) calculate the test variable V_i values for each percentage of time (preferred values are 0.001, 0.002, 0.003, 0.005, 0.01, 0.02, 0.03, 0.05, and 0.1), take into account a weighting function and calculate the mean $\overline{\mu}_V$, standard deviation $\overline{\sigma}_V$ and r.m.s. value $\overline{\rho}_V$ of all these V_i values over the required decades of probability levels.

5. Measured Data and Predictions

The following subsections present comprehensive statistics of three years measured data and predicted rain attenuation from 2014 to 2016.

5.1. Measured rain and attenuation distributions

To get a sense of the climatic conditions in the three years of measurements, the measured rain rate and attenuation at the three sites are shown from **Figure 4** to **Figure 9**. In these figures all rain data has been used and averaged for three years assuming zero rain during outage periods.

5.1.2. Rain rate and attenuation Røst

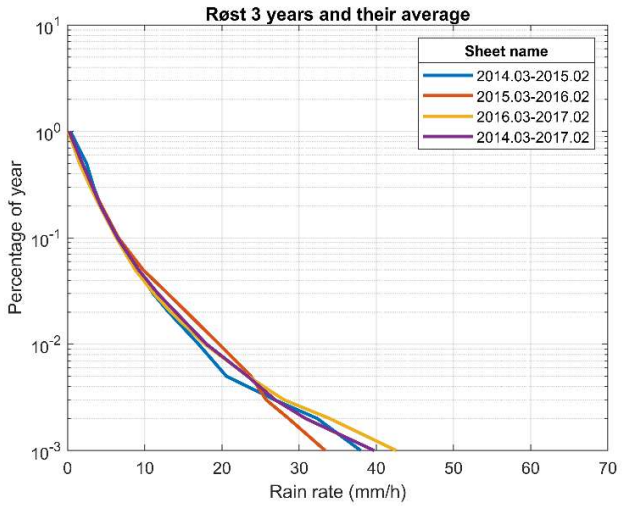

Figure 8: Measured rain rate at Røst.

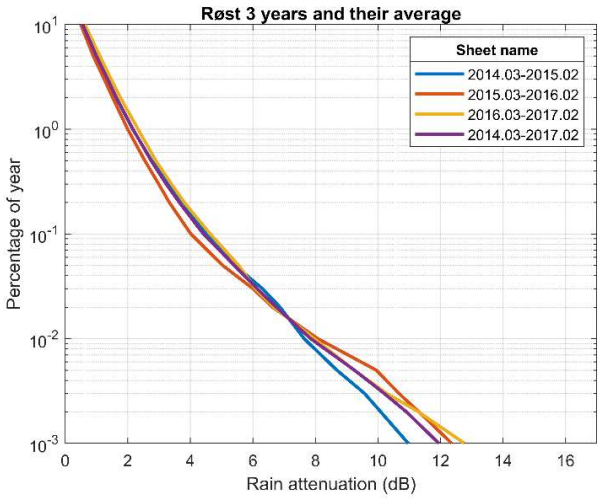

Figure 9: Measured rain attenuation at Røst.

Røst is a minuscule island in the middle of the sea, with little variation in temperature and rain intensity during the year. Convective rain is nearly inexistent in contrast moderate intensity stratiform rain happen frequently. Consequently, a significant proportion of low amplitude attenuation and virtually no yearly or monthly variation hold true (Tjelta et al., 2017 [13]).

5.1.3. Rain rate and attenuation Nittedal

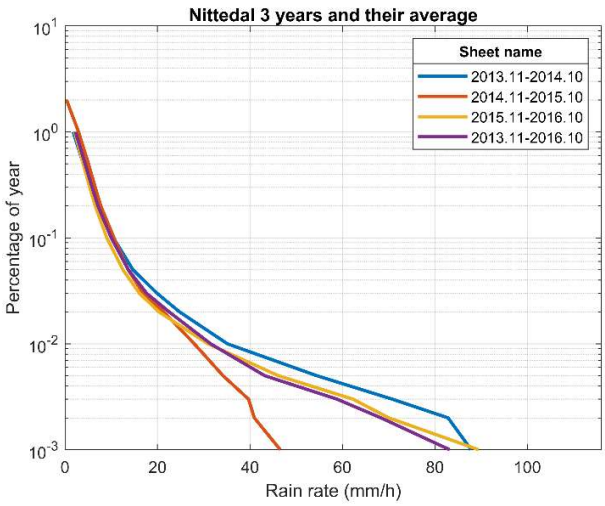

Figure 10: Measured rain rate at Nittedal.

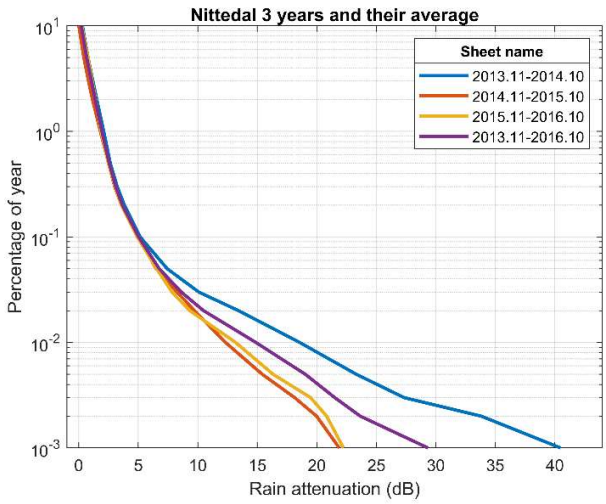

Figure 11: Measured rain attenuation at Nittedal.

Nittedal possesses inland climate coupled with extensive convective rain events throughout the summer months that culminates in high attenuation (Tjelta et al., 2017 [13]).

5.1.4. Rain rate and attenuation Vadsø

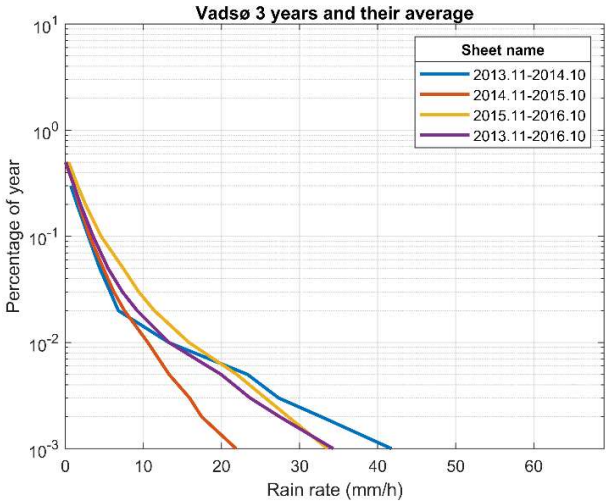

Figure 12: Measured rain rate at Vadsø

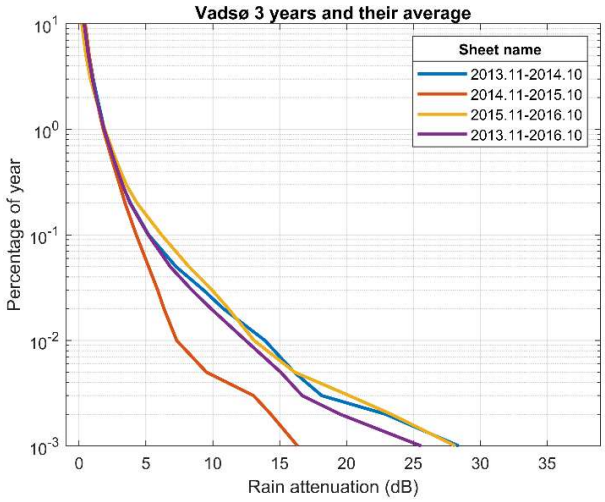

Figure 13: Measured rain attenuation at Vadsø

Owing to a modest elevation angle at Vadsø, even the moderate-intensity rain registered results in relatively sizable attenuation. Moreover, albeit the station is at the littoral of a small fjord, it is hedged by an important landmass. Hence, amid summertime there are convective high-intensity occurrence that induce large attenuation (Tjelta et al., 2017 [13]).

.

5.2. Comparison of Measured and Predicted Attenuation

5.2.1. Average measured and predicted attenuation Nittedal

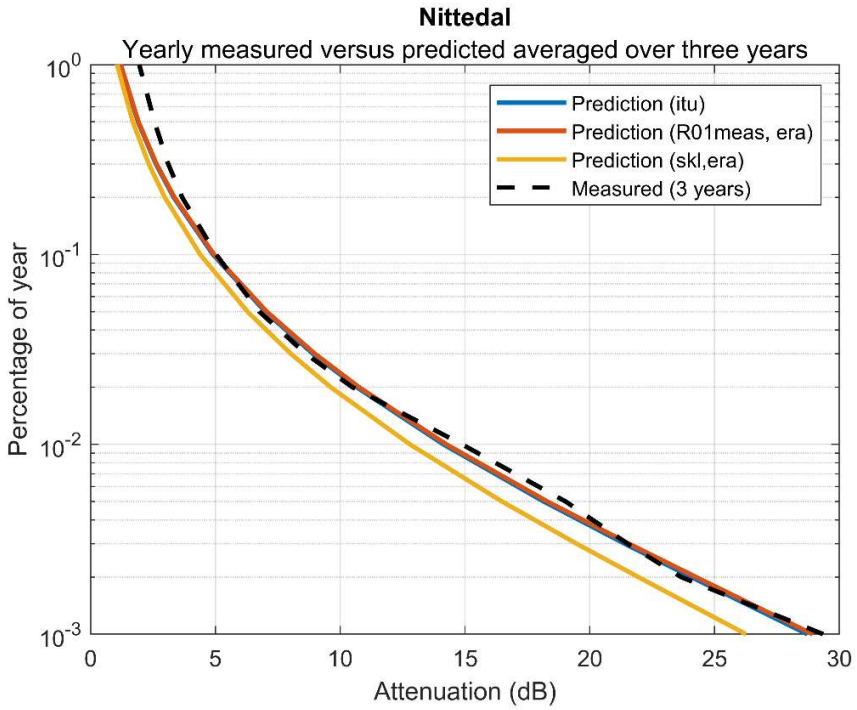

Figure 14: CCDF of average three-year measured rain attenuation compared with predictions for Nittedal.

In this section, a three-year average of measured rain attenuation data is compared with three sets of predicted rain attenuation data. The first set is a rain attenuation prediction using ITU-R tabulated data, followed by a data set representing the rain attenuation prediction using measured rain rate and rain height from ERA5, and the third set of data is the prediction using rain height from ERA5 and SEKLIMA local data, which uses climate data service provided by met.no from a nearby location, Hakadal in the case of Nittedal.

The CCDF's investigation of the three annual predicted attenuations, averaged over three years shown in **Figure 14**, reveals that the predictions seem to follow the same trend as the three years attenuation measured at Nittedal.

5.2.1.1. Monthly measured and predicted attenuation Nittedal

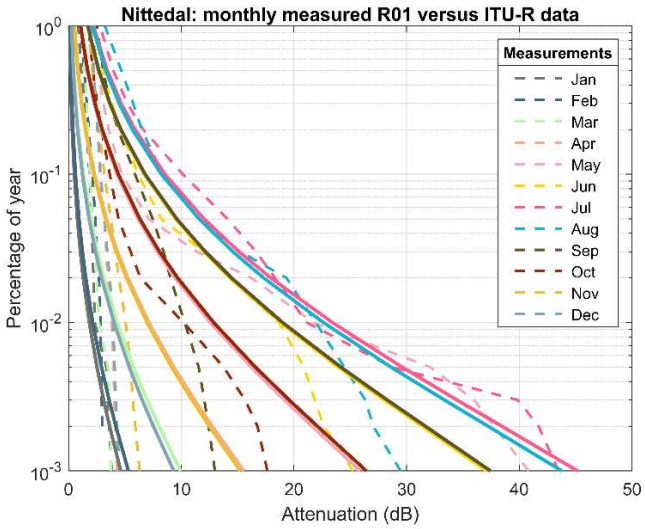

Figure 15a: Average three year monthly measured attenuations compared to monthly predicted attenuations using ITU-R data for Nittedal.

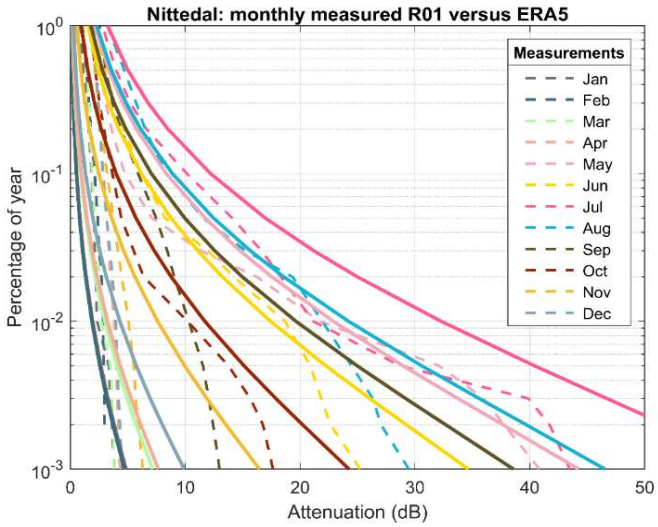

Figure 15b: Average three year monthly measured attenuations compared to monthly predicted attenuations using ERA5 data for Nittedal.

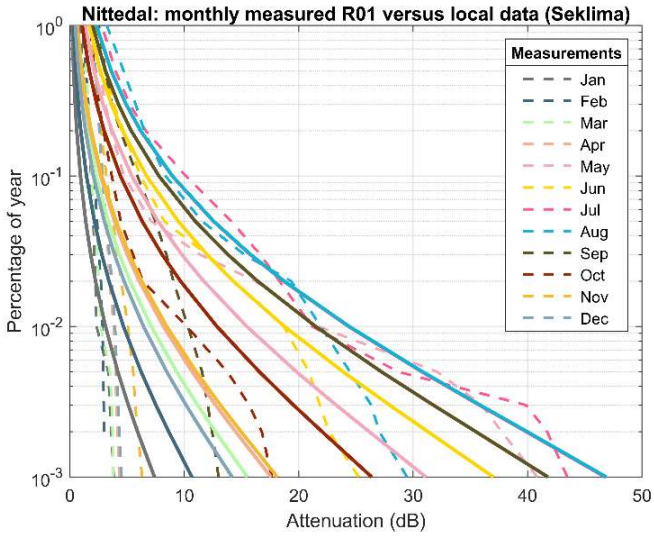

Figugure 15c: Average three year monthly measured compared to monthly predicted attenuations using local SEKLIMA data for Nittedal.

The comparison of monthly measured and predicted attenuation is shown in **Figure 15 (a** - c**)**. In order to be able to determine how well the predicted attenuation model fit the measured data, we have calculated the prediction using three set of data, that is ITU-R, ERA5, and SE KLIMA respectively.

For the case of Nittedal, **Figure 15a** show that the monthly predicted attenuation model using ITU-R data captures trends in measured monthly attenuations with reasonable accuracy. For instance, the low and high attenuations due to rain correspond moderately.

In **Figure 15b** it is apparent that the monthly predicted attenuations model using ERA5 data shows a god fit at low attenuations, corresponding to months with low rain rates, while largely overestimating the measured attenuations at the month with high attenuation, namely July.

The model predicted with SE KLIMA data, in **Figure 15c** display poor concordance with measured data at low attenuations. These assessments will be discussed in more detail when we introduce the test-variable in the next paragraph.

5.2.1.2. Testing variable for verification of prediction Nittedal

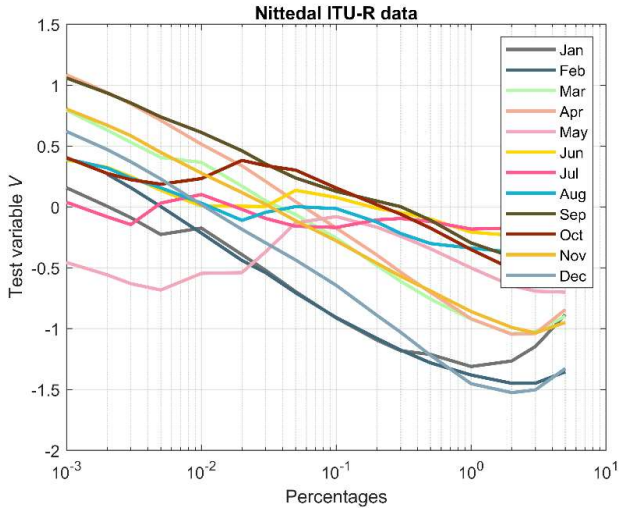

Figure 16a: Model validation using predicted ITU-R Rec. P.837 rain rates with ITU-R tabulated data and rain heights derived from ERA5 data for Nittedal.

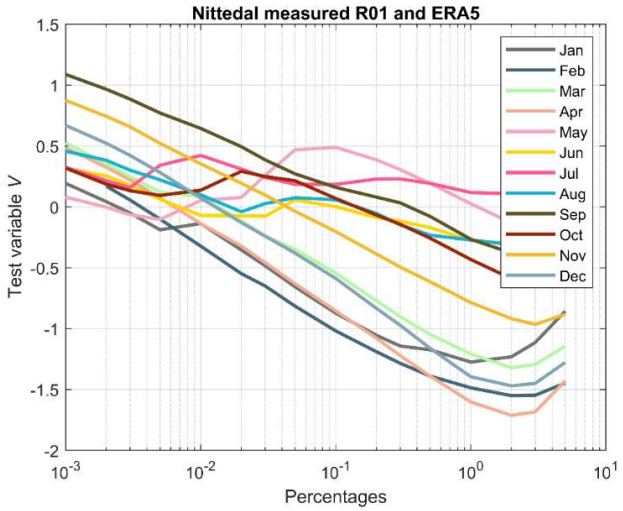

Figure 16b: Model validation using measured rain rates and rain heights provided by ERA5 database for Nittedal.

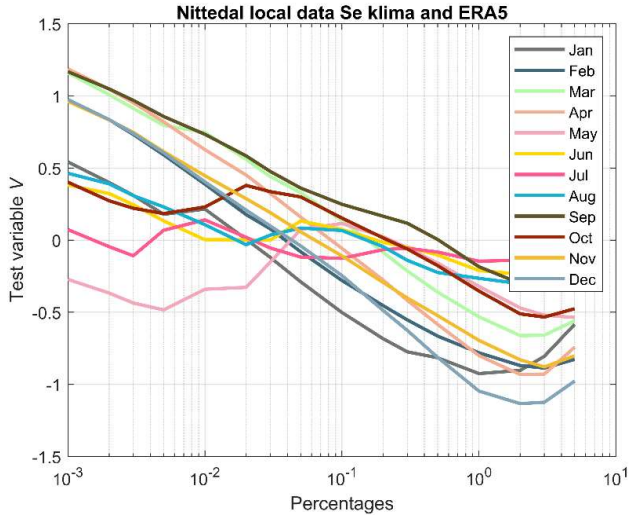

Figugure 16c: Model validation using predicted rain rates from ITU-R rec. P.837 using SEKLIMA local data and rain heights as for ERA5 for Nittedal.

In this section, comparison between measured attenuation values with our prediction model using the different data sets is performed in order to test the performance of our model. Note that when the measured values are equal to the predicted model, the values of the test variables are zero, which represents the best result.

The testing variable method defined by ITU-R fascicle [Nr.] is used and the results related to Nittedal are illustrated in **Figures 16a**, **16b** and **16c** respectively.

ITU-R data shown in **Figure 16a**, applies predicted rain rate (based on ITU-R recommendation P.837) using ITUR tabulated rainfall rates and rain heights from ERA5. Here, the summer months: June, July and August give the best performance in terms of test variable where the ratio between predicted and measured attenuation is close to zero from the probability of exceedance of 0.001% and more markedly at the probability of exceedance of 0.1%. When the percentage of exceedance increases from 0.1% to 1%, the values are slightly off the zero-test variable line but close enough to be considered acceptable, though not outstanding or perfect.

The values of the test variables for the remaining seasons, autumn, winter and spring are further spread out from the zero-test variable line at 0.001% and 0.1% probability exceedance and worsen as the exceedance percentage increases, revealing deterioration or a mismatch between predicted and measured attenuation values.

The same trend is observed for the datasets used as secondary sources for determining rainfall rate based on measured rain rates and rain heights from ERA5 shown in **Figure 16b** and the local SEKLIMA database which uses predicted rain rate from ITU-R rec.P.837 and the rain heights from ERA5 shown in **Figure 16c**, where the summer months are still close to the zero-test variable line while the remaining seasons are even further extended from the zero line. The test with measured rain rates and ERA5 rain heights data (Figure 14b) shows a large scatter at the probability of exceedance of 0.1% and more at 1% exceedance, while the test with the local SEKLIMA data has the highest dispersion at 0.001% and the smallest deviation at 0.1% and 1% of all scenarios, except for the summer months.

5.2.2. Average measured and predicted attenuation Røst

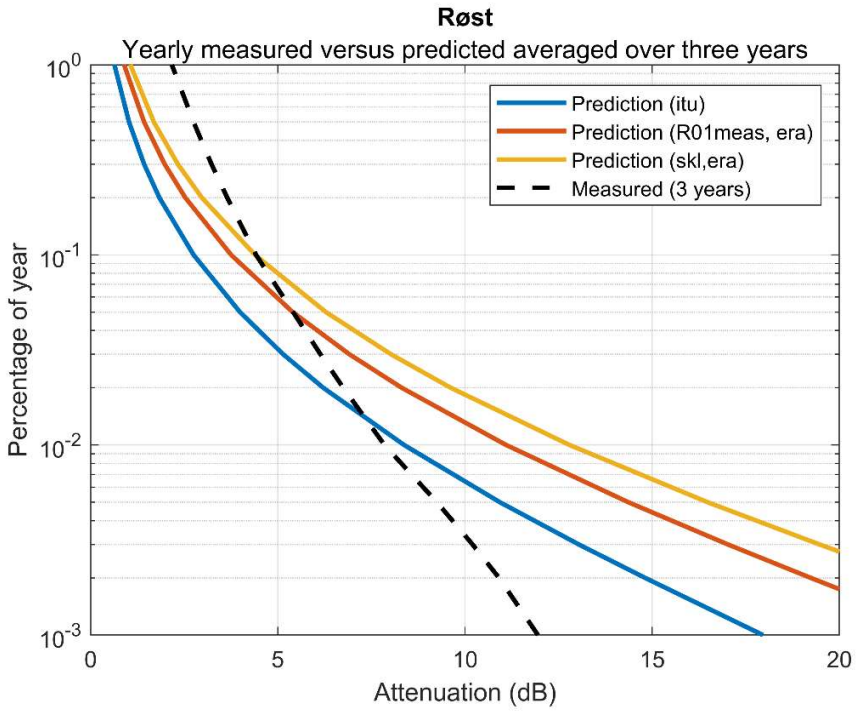

Figure 17: CCDF of average three-year measured rain attenuation compared with predictions for Røst.

For the experiment at Røst, the SEKLIMA local data used stem from the nearby location of Røst Lufthavn.

The CCDF's investigation of the three annual predicted attenuations, averaged over three years shown in **Figure 17**, reveals that the predictions do not follow the same trend as the three years attenuation measured at Røst.

5.2.2.1. Monthly measured and predicted attenuation Røst

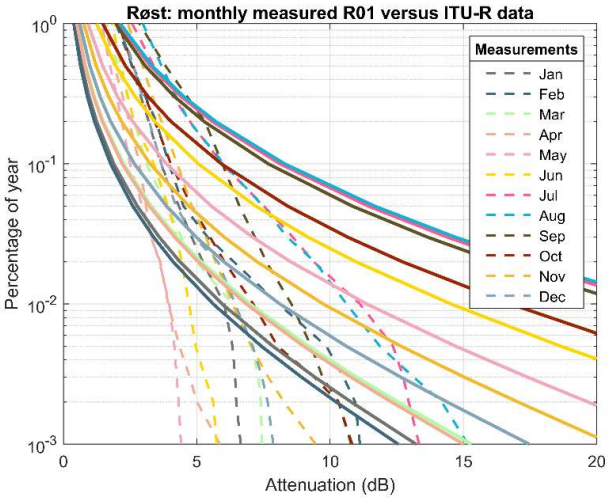

Figure 18a: Average three year monthly measured attenuations compared to monthly predicted attenuations using ITU-R data for Røst.

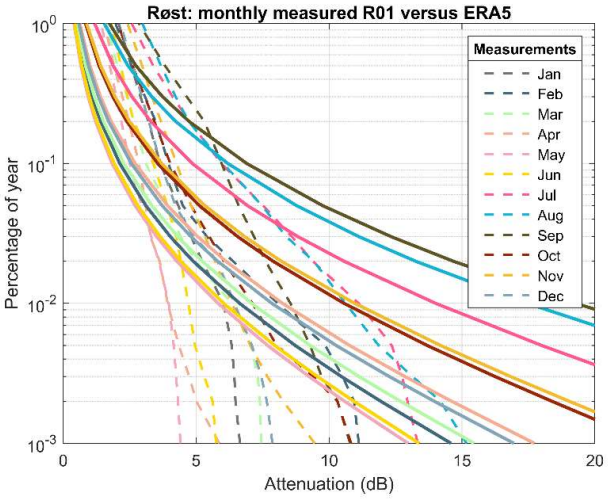

Figure 18b: Average three year monthly measured attenuations compared to monthly predicted attenuations using ERA5 data for Røst.

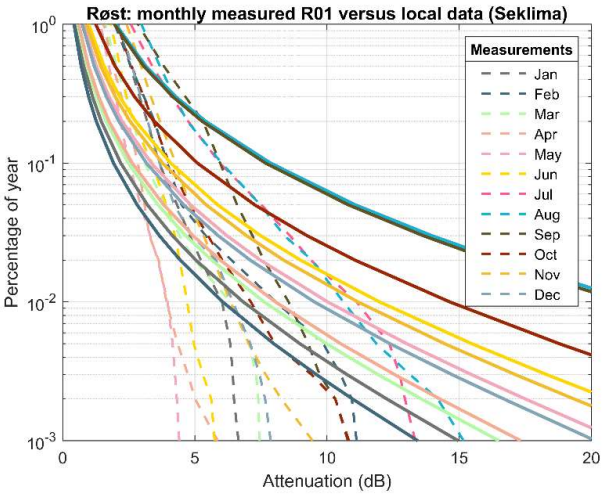

Figugure 18c: Average three year monthly measured compared to monthly predicted attenuations using local SEKLIMA data for Røst.

For Røst, **Figure 18a**, shows that the monthly predicted attenuation model using ITU-R data does not coincide with the trends in measured monthly attenuations.

Further investigation of the CCDF of the monthly predicted attenuations model using ERA5 data shown in **Figure 18b**, and that using SEKLIMA data in **Figure 18c**, do not follow the same distribution as the monthly measured rain attenuations.

5.2.1.3. Testing variable for verification of prediction Røst

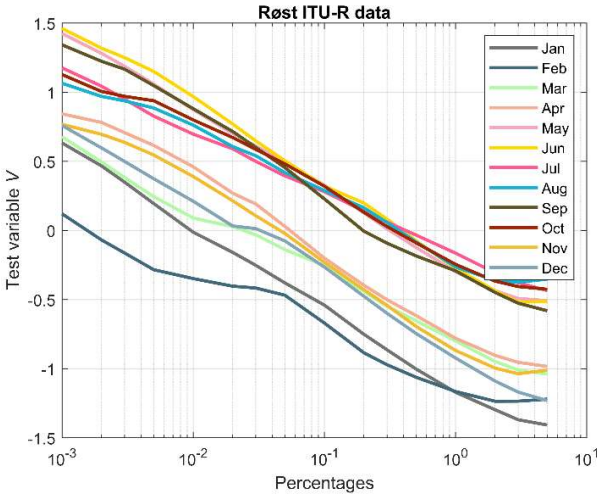

Figure 19a: Model validation using predicted ITU-R Rec. P.837 rain rates with ITU-R tabulated data and rain heights derived from ERA5 data for Røst.

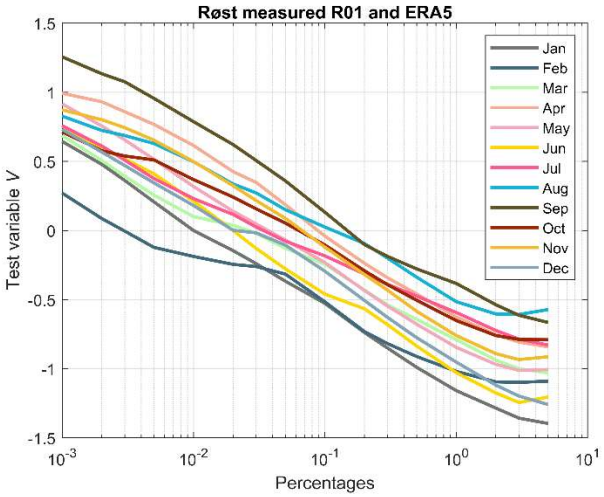

Figure 19b: Model validation using measured rain rates and rain heights provided by ERA5 database for Røst.

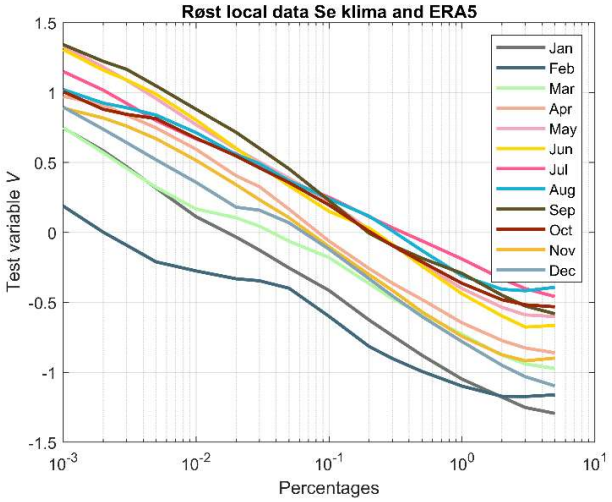

Figugure 19c: Model validation using predicted rain rates from ITU-R rec. P.837 using SEKLIMA local data and rain heights as for ERA5 for Røst.

Model validation for verification of the predicted attenuation at Røst is shown in **Figures 19 (a - c).** The salient point to retain from this investigation is that none of the monthly test-variable lines parallel the zero-line (concordance line), they all cross the zero-line revealing a non-concordance between measurements and predictions for each month. Since for each percentage of time the test-variable is calculated as the natural logarithm of the ratio of the predicted attenuation to the measured attenuation, the positive test-variable at the 0.001% probability level shows an overestimation of the predicted values compared to the measured values, due to poor performance of our model, whilst values below the zero-line at 1% probability level count as underestimated prediction values, which is also an indication of mediocre model performance.

At 0.01% probability, the ITU-R data using predicted rain rate and ITU tabulated rain height data from ERA5, **Figure 19a**, shows a split dispersion with half of the test-variable values above the zero-line and the other half appearing below the zero-line. At 1% all the test-variables are located below the zero-line, hence their negative values.

In **Figure 19b**, where data with measured rain rate and rain height from ERA5 are used, shows less dispersion at 0.001%, 0.1% and 1% probability levels of all scenarios studied.

Data utilizing predicted rain rate using local SEKLIMA data and rain height from ERA5 shown in **Figure 19c**, exhibit almost the same results as in **Figure 19a**.

5.2.3. Average measured and predicted attenuation Vadsø

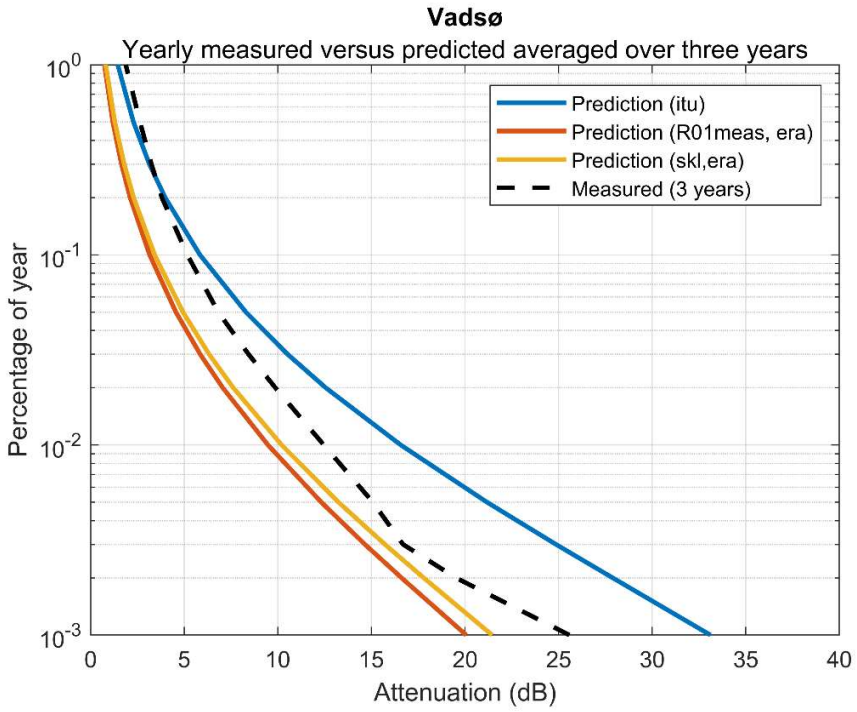

Figure 20: CCDF of average three-year measured rain attenuation compared with predictions for Vadsø.

For the case of Vadsø, **Figure 20** shows a nearly perfect alignment between the three-year averaged annual prediction using ITU data and the measured data for the same period, however, this alignment only exists at the small interval of 0 dB to 5 dB, afterward the two distributions gradually split.

Considering the two remaining predictions, one using measured rain rate and ERA5 rain height and the other using local SEKLIMA data and ERA5 rain height, their CCDF distribution path appears to be parallel to the measurement data, although they do not align with these.

For the Vadsø experiment, the local SEKLIMA data used comes from the neighboring locality of Tana Bru.

5.2.3.1. Monthly measured and predicted attenuation Vadsø

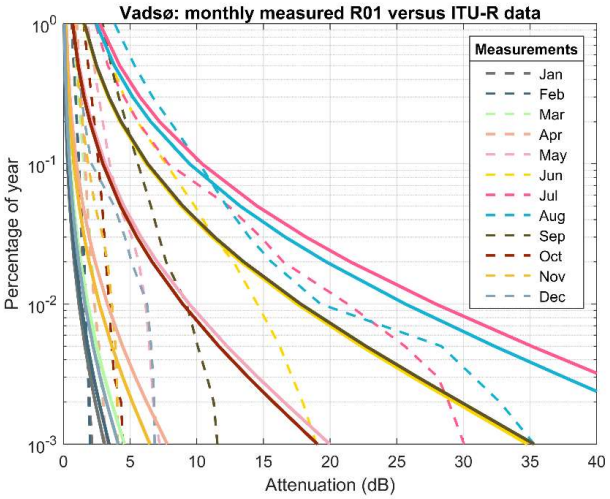

Figure 20a: Average three year monthly measured attenuations compared to monthly predicted attenuations using ITU-R data for Vadsø.

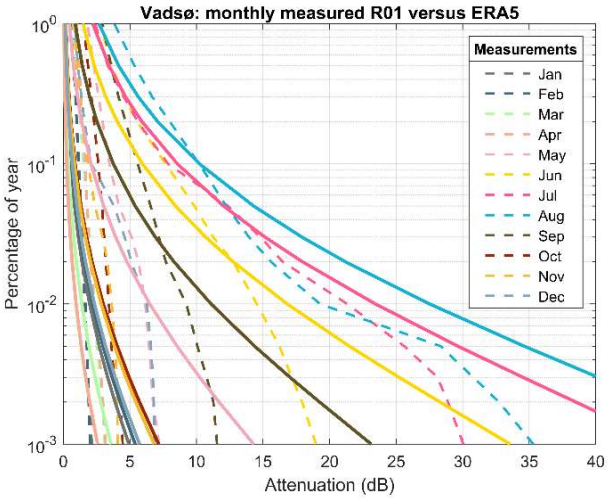

Figure 20b: Average three year monthly measured attenuations compared to monthly predicted attenuations using ERA5 data for Vadsø.

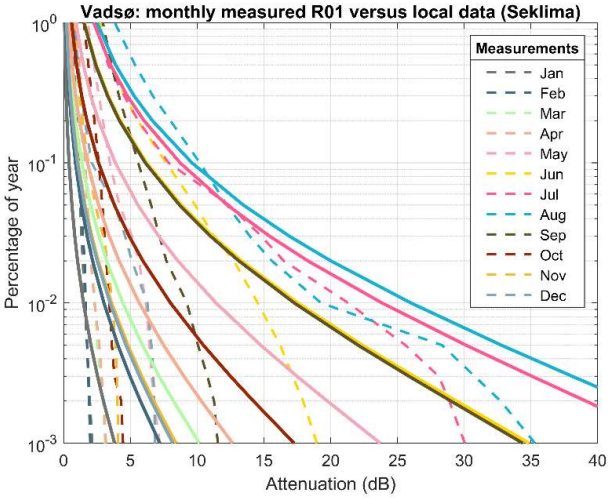

Figugure 120c: Average three year monthly measured compared to monthly predicted attenuations using local SEKLIMA data for Vadsø.

All three datasets show a somewhat similar trend between predicted monthly attenuation and measured monthly attenuation at 1% of the year down to 0.1% of the year. As the percentage decreases towards 0.01% and 0.001% of the year the dispersion is more noticeable.

For the three scenarios, it can be noted that for July and August (summer season), the predictions seem to follow the measurements up to the attenuation value of around 15 dB, the trend is more pronounced for July in **Figures 20b** and **20c**.

At this stage it is premature to give an assessment of the performance of the model on the Vadsø experiment, but at a quick glance one could say that from 1% to 0.1% of the year the model could give a satisfactory prediction for the month of July in Vadsø, when prediction is based on data employing measured rain rate and rain height from ERA5, also when it uses data SEKLIMA data and ERA5's rain height, but this claim needs to be verified by the model validation which follows in the next paragraph.

5.2.3.2. Testing variable for verification of prediction Vadsø

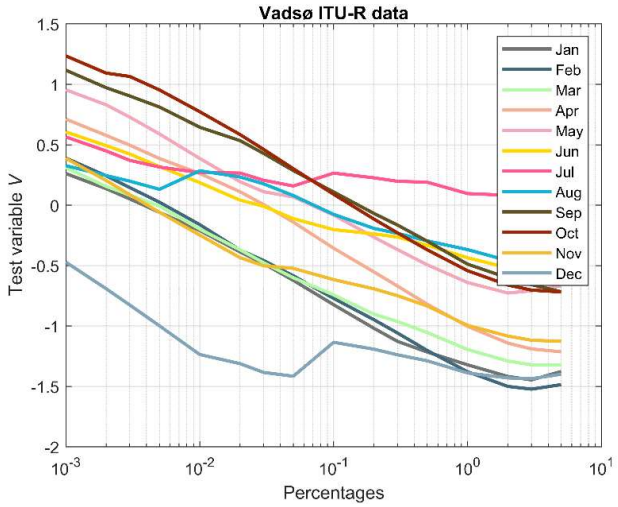

Figure 21a: Model validation using predicted ITU-R Rec. P.837 rain rates with ITU-R tabulated data and rain heights derived from ERA5 data for Vadsø.

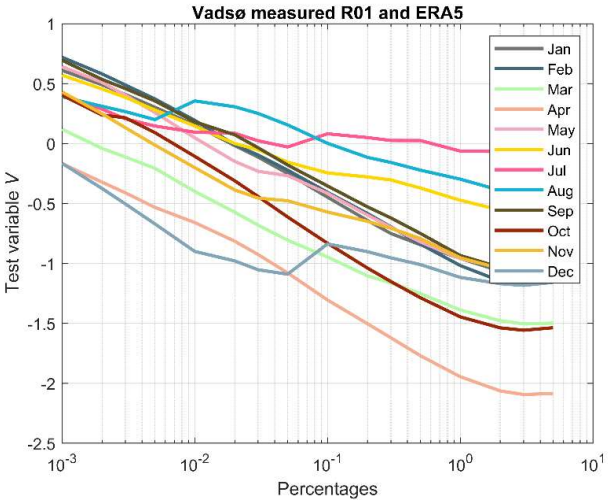

Figure 21b: Model validation using measured rain rates and rain heights provided by ERA5 database for Vadsø.

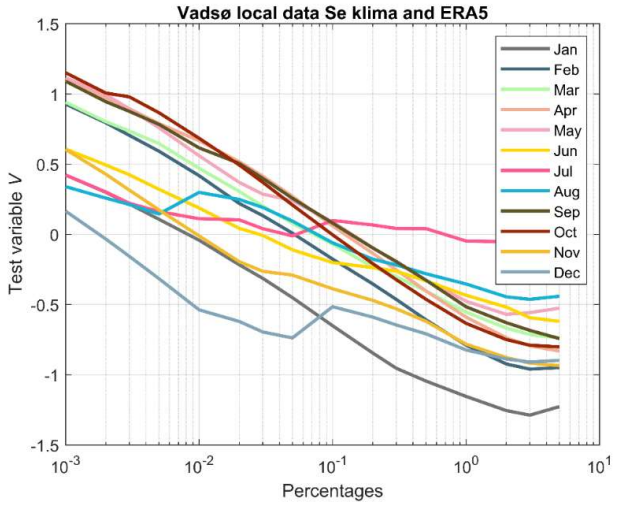

Figugure 21c: Model validation using predicted rain rates from ITU-R rec. P.837 using SEKLIMA local data and rain heights as for ERA5 for Vadsø.

For Vadsø, the **Figures 21 (a -c)** show that only the test-variable for July appears consistently parallel to the zero-line although it is not completely aligned with it. The best alignment on the zero-line is observed from 0.1% to 1% in **Figures 21b** and **21c**. Ultimately, this is not a good performance for our prediction model for Vadsø, since the test-variables of the remaining months are all spread further from the zero-line, indicating a non-conformity between the measured monthly attenuation and the predicted monthly attenuation.

6. Conclusion and Suggestions for future work

6.1. conclusion

The model was implemented with three-year propagation data from three sites in Norway, with elevation angles stretching from 10.1° to 21.8°. The first site, Nittedal, has a continental environment, the second site, Røst, has a maritime (island) surroundings, and the third site, Vadsø, has arctic conditions. A satellite operating at 19.7 Ghz frequency was the focus of attention because rain attenuation at this frequency is a serious issue and must be examined for any link budget analysis.

The development of a prediction model to predict monthly rain attenuation relied on two main components, rainfall rate and rain height. In order to determine how well the developed model fits the measured data, three datasets were employed. The first dataset uses rain rate distribution derived from ITU-R maps and rain height from ERA5, the second dataset uses a measured rain rate and rain height from ERA5, while the third set of data applies rain rate from local SEKLIMA data and the rain height from ERA5.

The prediction model was tested against measured data for the selected sites. The test showed that the model performs best at Nittedal measurement site during the summer months: June, July and August in terms of test-variable where the ratio between predicted and measured attenuation is close to a log zero from the probability of exceedance of 0.001% to the probability of exceedance of 0.1%. When the percentage of exceedance increases from 0.1% to 1%, the values are slightly off the zero-test variable line, but close enough to be considered acceptable, though not outstanding or perfect. Outside the summer months, the model performed quite poorly. In terms of dataset used, there is not a big difference, except for the fact that the test-variable for July seems to follow the zero-line better with the prediction using ITU-R data (first dataset) and local SEKLIMA data (third dataset), the reason could be that these datasets have been collected for many years.

For Røst and Vadsø, a good agreement was not found in the comparison of the measured rain attenuation with our prediction model. It should be noted that the predicted annual attenuation compared to the measured annual attenuation showed a poor performance for these two measurement sites, perhaps if the annual prediction agreed with the measurement, we could have had a better performance for the monthly predictions for Røst and Vadsø as well. For attenuation above 10 dB or so, the yearly prediction is quite bad for Røst. For

Vadsø, not as bad as Røst, but worse than Nittedal. For Vadsø, it may seem that the annual method works quite well for July.

6.2. Suggestions for future work

The result indicates that if the prediction method for one year works, then the method for summer also works, especially for Nittedal, but not for other seasons.

The variation for Røst is smaller than the other two places. The result is unclear with regards to whether, an annual method will work for months for Røst, but as the deviation is, it is conceivable that a revised annual method would also work well for months for Røst.

BIBLIOGRAPHY

[1] C. Capsoni, L. Luini, A. Paraboni, C. Riva, A. Martellucci. ***"A new prediction model of rain attenuation that separately accounts for stratiform and convective rain".*** IEEE Transactions on Antennas and Propagation, Vol 57, No. 1, January 2009, Page(s): 196 - 204.

[2] Kolawole, Michael O. *"**Satellite Communication Engineering**"*. CRC Press, 2002.

[3] Ippolito Jr., Louis J**. *Radiowave "Propagation in Satellite Communications***". Springer Netherlands, 1986.

[4] ***Norwegian Participation in Space and Satellite Activities***. Lecture by Pål Brekke, Norwegian Space Center, 2020.

[5] ***A Satellite System for Broadband Communications to Polar Area***. Thesis by Lars Løge, NTNU, 2008.

[6] ITUR. *"**Recommendation ITU-R P-618-13**"*. ITU, 2017.

[7] https://www.britannica.com/science/space-weather/Effects-on-satellite-communications-and-navigation.

[8] https://www.britannica.com/science/lapse-rate

[9] ITUR. *"**Recommendation ITU-R P-837-7**"*. ITU, 2017.

[10] https://www.besttravelmonths.com/norway/nittedal-2946448/

[11] [**Martin Hall & Les Barclay**]. ***[Propagation of Radiowaves 2nd Ed.]***. [**The Institution of Engineering and Technology, London, UK**], [**year of publication**].

[12] **https://cds.climate.copernicus.eu/cdsapp#!/dataset/10.24381/cds.f17050d7?tab=overview**

[13] Tjelta, Bråten, Håkegård, Grotthing, Rytir, Cheffena, Grythe. ***"Ka-band Radio Characterization for SatCom Services in Arctic and High***

Latitude Regions". European Space Agency, 2017.

[14] **Fascicle on Testing Variables Used for the Selection of Prediction Methods.** ITU Radiocommunication Study Groups, 2016.

[15] https://www.climatestotravel.com/climate/norway/rost

[16] https://weatherspark.com/y/96282/Average-Weather-in-Vads%C3%B8-Norway-Year-Rou